PAPER

Check for updates

Improving printability of hydrogel-based bio-inks for thermal inkjet bioprinting applications *via* saponification and heat treatment processes†

Ratima Suntornnond,[a] Wei Long Ng, ⓘD *[a] Xi Huang,[a] Chuen Herh Ethan Yeow[a] and Wai Yee Yeong ⓘD *[ab]

Material jetting bioprinting is a highly promising three-dimensional (3D) bioprinting technique that facilitates drop-on-demand (DOD) deposition of biomaterials and cells at pre-defined positions with high precision and resolution. A major challenge that hinders the prevalent use of the material jetting bioprinting technique is due to its limited range of printable hydrogel-based bio-inks. As a proof-of-concept, further modifications were made to gelatin methacrylate (GelMA), a gold-standard bio-ink, to improve its printability in a thermal inkjet bioprinter (HP Inc. D300e Digital Dispenser). A two-step modification process comprising saponification and heat treatment was performed; the GelMA bio-ink was first modified *via* a saponification process under highly alkali conditions to obtain saponified GelMA (SP-GelMA), followed by heat treatment *via* an autoclaving process to obtain heat-treated SP-GelMA (HSP-GelMA). The bio-ink modification process was optimized by evaluating the material properties of the GelMA bio-inks *via* rheological characterization, the bio-ink crosslinking test, nuclear magnetic resonance (NMR) spectroscopy and the material swelling ratio after different numbers of heat treatment cycles (0, 1, 2 and 3 cycles). Lastly, size-exclusion chromatography with multi-angle light scattering (SEC-MALS) was performed to determine the effect of heat treatment on the molecular weight of the bio-inks. In this work, the 4% H2SP-GelMA bio-inks (after 2 heat treatment cycles) demonstrated good printability and biocompatibility (in terms of cell viability and proliferation profile). Furthermore, thermal inkjet bioprinting of the modified hydrogel-based bio-ink (a two-step modification process comprising saponification and heat treatment) *via* direct/indirect cell patterning is a facile approach for potential fundamental cell–cell and cell–material interaction studies.

1. Introduction

3D bioprinting is a highly automated and advanced technology that facilitates the fabrication of complex and biomimetic 3D tissue-engineered constructs.[1–6] It enables the precise patterning of living cells and biomaterials *via* a layer-by-layer fabrication approach to control the spatial arrangement of these functional components to achieve optimal cell–cell and cell–biomaterial interactions.[7–10] The 3D bioprinting techniques can be categorized into 3 distinct processes: material jetting,[11–16] material extrusion[17–20] and vat polymerization.[21–23] These bioprinting techniques have their specific advantages and limitations and the choice of a suitable bioprinting technique should be dependent on the intended application. The drop-on-demand (DOD) material jetting bioprinting technique (inkjet bioprinting,[24] microvalve bioprinting[25] and laser-assisted bioprinting[26]) enables contactless patterning and deposition of different types of biomaterials and living cells within each layer, which is critical for achieving improved cell–cell and cell–matrix interactions within the 3D tissue-engineered constructs.[27–31]

Most of the existing bio-inks for bioprinting techniques are hydrogel-based bio-inks with good biocompatibility that facilitate cell encapsulation and support cell proliferation over time.[32,33] These bio-inks include collagen-based,[34–37] gelatin-based,[38–41] fibrin-based,[42,43] hyaluronic acid-based,[44,45] silk fibroin[46,47] and so on. To date, the gelatin methacrylate (GelMA) bio-ink is widely used due to its tunable mechanical properties, controllable degradation rate and good biocompatibility.[48–50] The gelatin component is a hydrolyzed form of

[a] HP-NTU Digital Manufacturing Corporate Lab, Nanyang Technological University (NTU), 65 Nanyang Avenue, 637460, Singapore. E-mail: ng.wl@ntu.edu.sg, wyyeong@ntu.edu.sg

[b] Singapore Centre for 3D Printing (SC3DP), School of Mechanical and Aerospace Engineering, Nanyang Technological University (NTU), 50 Nanyang Avenue, 639798, Singapore

† Electronic supplementary information (ESI) available. See DOI: https://doi.org/10.1039/d2tb00442a

This journal is © The Royal Society of Chemistry 2022

J. Mater. Chem. B, 2022, **10**, 5989–6000 | 5989

collagen which contains cell-signaling motifs such as arginine–glycine–aspartic acid (RGD) sequences that facilitate cell attachments and target sequences of matrix metalloproteinase (MMP) that is critical for cellular remodeling. GelMA is considered a gold-standard bio-ink for bioprinting applications and it is formed *via* a reaction between gelatin and methacrylic anhydride to confer the photo-crosslinking properties[51,52] which enhances the overall mechanical properties of the gelatin and leads to a controllable degradation rate.[53]

A major limitation that hinders the prevalent use of material jetting bioprinting approaches is due to its limited choice of printable bio-inks. Among the various material jetting bioprinting approaches, the inkjet bioprinting technique has the most stringent requirements for a printable bio-ink, which include the bio-ink viscosity, surface tension and density.[54,55] The drop-on-demand (DOD) inkjet bioprinting techniques can be classified as thermal/piezoelectric/electrostatic inkjet bioprinting; the thermal actuator in thermal inkjet bioprinting locally heats the bio-ink to form a vapor bubble that expands and collapses rapidly to generate a pressure pulse within the fluid chamber, whereas the piezoelectric/electrostatic actuator changes its shape to displace the bio-ink within the fluid chamber to generate a pressure pulse. Furthermore, it has been reported that the inkjet bioprinting techniques do not have significant influence on the cell viability ($\sim$80–90% cell viability after printing).[11] Although the thermal inkjet print-head can only be used to deposit a narrower range of bio-inks, it is much cheaper to manufacture and can be packed at a higher density per printer as compared to the piezoelectric/electrostatic inkjet print-head to achieve significantly higher printing throughput.[11] Hence, the envisioned goal was to perform further modifications to GelMA bio-inks in this proof-of-concept study to reduce its long molecular chains (which leads to high viscosity) and improve its printability in a thermal inkjet print-head.

Our study demonstrated that a two-step modification process comprising saponification and heat treatment helped in improving the printability of the GelMA bio-ink in the thermal inkjet print-head significantly. An optimal heat treatment process of 2 cycles resulted in a significant decrease in the viscosity of the bio-ink and the molecular weight to improve its printability while retaining its ability to undergo both physical crosslinking and chemical crosslinking. The encapsulated cells within the modified GelMA bio-inks remained viable and continued to proliferate well over a period of 7 days; direct/indirect cell patterning can be performed in a facile manner for potential fundamental cell–cell and cell–material interaction studies.

2. Materials and methods

2.1. Bio-ink synthesis and modification

Gelatin methacrylate (GelMA) was synthesized following a previously reported protocol.[56] Briefly, 10 g of gelatin type A, from porcine skin, with a gel strength of 300 bloom (Sigma-Aldrich, G2500) was solubilized in pre-heated sterile 1$\times$ phosphate buffered saline (PBS) to reach a final concentration of 10% w/v. This mixture was stirred at 50 °C inside a chemical safety fume hood until the solution appeared clear and homogenous. Methacrylic anhydride (MAAh) (Sigma-Aldrich, USA, 276685) was added dropwise to the gelatin solution (0.6 g of MAAh per gram of gelatin) and stirred at 500 rpm for 3 hours at 50 °C to facilitate the functionalization of gelatin with photo-curable methacrylate groups. The resultant gelatin methacrylate solution was then aliquoted to 50 ml falcon tubes and centrifuged at 3000 $\times$ *g* for 5 minutes to pellet the unreacted MAAh. The supernatant was diluted two times the volume by using 1$\times$ PBS at 40 °C. The solution was dialyzed for seven days against distilled water at 40 °C through a 12–14 kDa cut-off dialysis membrane (Sigma-Aldrich, USA).

A two-step modification process comprising saponification and heat treatment was performed; the GelMA bio-ink was first modified *via* the saponification process under highly alkali conditions to obtain saponified GelMA (SP-GelMA), followed by heat treatment *via* the autoclaving process to obtain heat-treated SP-GelMA (HSP-GelMA) (Fig. 1). The saponification process was performed according to a previous protocol[57] by adding 10 M sodium hydroxide (NaOH) to the dialyzed solution to obtain a final pH of 11 over a period of 15 minutes prior to a neutralization process using 10% v/v acetic acid to obtain the saponified GelMA (SP-GelMA). The SP-GelMA solution was then lyophilized over a period of 7–10 days until it turned into solid white foam and stored at −30 °C until further use.

Prior to use, the SP-GelMA solution required an additional post-saponification step by treating SP-GelMA in 1$\times$ PBS with 0.09 M NaOH for 30 minutes and adjusting the pH back to 7.4 with 10% v/v acetic acid. Next, SP-GelMA was heat-treated *via* an autoclaving process at 121 °C and 15 psi over different heat-treatment cycles (1–3 cycles) to obtain the heat-treated SP-GelMA (HSP-GelMA). The HSP-GelMA solution was sterile filtered using a 0.22 μm pore filter, Merck Millipore Stericup™ Sterile Vacuum Filter Units. The filtered HSP-GelMA solution was then adjusted to the 4% w/v concentration and kept inside a 37 °C oven for 1–2 days before bioprinting. The HSP-GelMA bio-inks used in this study are denoted as H$\times$SP-GelMA, where $\times$ represented the number of heat treatment cycles (0, 1, 2 and 3 cycles).

2.2. Bio-ink characterization

2.2.1. Material printability. In this study, a thermal inkjet printer (HP D300e Digital Dispenser) was utilized for bio-ink printing using non-commercial cell-printing cassettes (prototype T8 cassettes with 8 embedded thermal inkjet print-heads with a large nozzle orifice diameter to enable cell printing) with a high printing frequency of 1 kHz. The thermal inkjet print-head dispensed a constant droplet volume of $\sim$0.345 nl and multiple droplets were printed at the same spot to achieve the desired droplet volume. The droplets were dispensed into a tissue-cultured well plate and hence the nozzle to the substrate distance is approximately 15 mm (the distance is dependent on the thickness of the well plate). The HP D300e digital dispenser was used to evaluate the printability of different H$\times$SP-GelMA
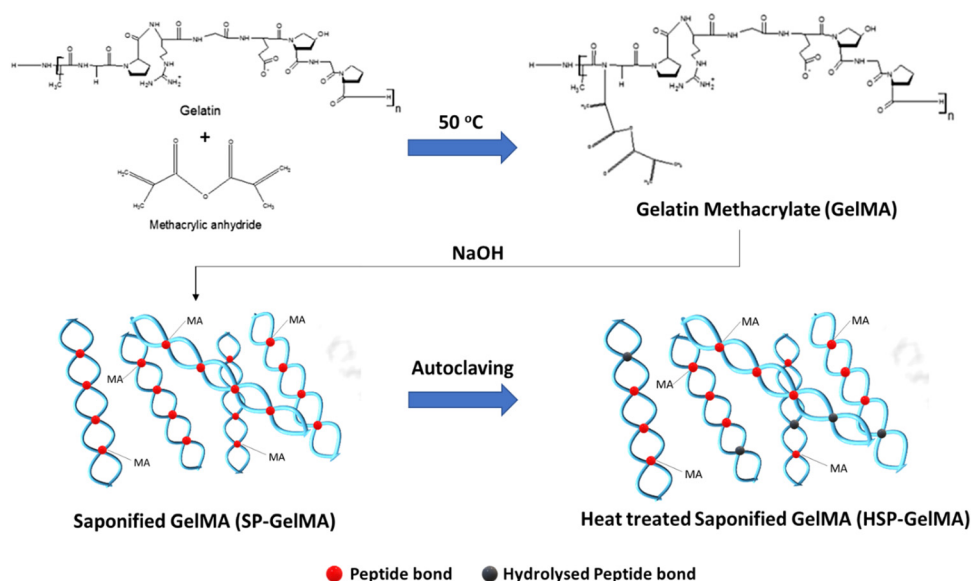
5990 | *J. Mater. Chem. B*, 2022, **10**, 5989–6000

This journal is © The Royal Society of Chemistry 2022

Fig. 1 Schematic drawing of the two-step modification process for the gelatin methacrylate (GelMA) bio-ink; a saponification process was first performed under highly alkali conditions, followed by the autoclaving process (different numbers of heat treatment cycles) to obtain the heat-saponified GelMA (HSP-GelMA) bio-inks which were illustrated in the macromolecular form.

bio-inks (where × varies from 0 to 3); the bio-inks were printed as 4 × 4 droplet arrays with a total dispensed volume of 20 nL per spot onto 24-well tissue culture plates.

2.2.2. Rheological characterization. The rheological properties of the H×SP-GelMA bio-inks (where × varies from 0 to 3) were evaluated using a discovery hybrid rheometer (TA Instruments, New Castle, DE, USA). The values of the strain amplitude were first verified to ensure that all measurements were performed within the linear viscoelastic region. Next, the viscosities of different HSP-GelMA bio-inks (0, 1, 2 and 3 cycles) were evaluated for shear rates ranging from 10^2 to 10^4 s^{-1} at a constant temperature of 25 °C. For the temperature sweep, the experiment was performed from 4 °C to 40 °C at 2 °C min^{-1} ramp rate and a constant angular frequency of 10.0 s^{-1}.

2.2.3. Bio-ink crosslinking test. Different bio-ink crosslinking tests were performed to evaluate the influence of heat treatment cycles on physical and chemical crosslinking properties. The physical crosslinking test was performed by pipetting different H×SP-GelMA bio-inks (where × varies from 0 to 3) at a constant volume of 20 μl onto the 24-well plates (n = 3 for each type of bio-ink) and submerging the various bio-inks in ice cold water (below 4 °C for 15 minutes) to observe the change in the sol–gel phase of the samples. The chemical crosslinking test was performed by pipetting different H×SP-GelMA bio-inks (where × varies from 0 to 3) at a constant volume of 20 μl onto the 24-well plates (n = 3 for each type of bio-ink) and crosslinking the various bio-inks in a UV flood curing system (Techno Digm, Singapore) operating at a 50% power intensity for 120 seconds to observe the change in the sol–gel phase of the samples.

2.2.4. Nuclear magnetic resonance (NMR) spectroscopy. For ^{1}H-nuclear magnetic resonance spectroscopy (^{1}H-NMR), H×SP-GelMA bio-inks (where × varies from 0 to 3) were diluted to a concentration of 10 mg ml^{-1} and characterized by ^{1}H-NMR 400 MHz (AVANCE I, Bruker, Germany) in D$_2$O solvent (Sigma-Aldrich, USA) focused of the peaks at 1.8–2.0, 5.7–5.9, and 6.1–6.3 ppm for the methacrylate group. The percentage of the methacrylate group was calculated by comparing the height of the peak against the H0SP-GelMA peak (no heat treatment).

2.2.5. Material swelling test. H×SP-GelMA bio-inks (where × varies from 0 to 3) were casted into a circular disc (n = 3, ∅ = 5 mm, and height = 5 mm). After this, samples were lyophilized and kept at −30 °C before further experiments. Consequently, hydrogel samples were soaked in DI water for 4 hours to ensure that they were fully swollen, and the swell ratio of the hydrogel was calculated by using the formula below in eqn (1):

$$\text{Swelling ratio} = \frac{W_{\text{swollen}} - W_{\text{dry}}}{W_{\text{dry}}} \times 100\% \qquad (1)$$

2.2.6. Size-exclusion chromatography with multi-angle light scattering (SEC-MALS). The molecular weights (M_w) of pristine GelMA and H×SP-GelMA bio-inks (where × varies from 0 to 2) were measured using a high performance liquid chromatography (HPLC) system with UV and a fluorescence detector that used size exclusion chromatography (SEC) (Shimadzu HPLC Prominence) with an S200 5/150GL column to separate samples. The eluted peaks were analyzed using a DawnHeleos-II Multi-Angle Light Scattering (MALS) detector to determine the weight average molecular weight (M_w), number average molecular weight (M_n), and polydispersity index (M_w/M_n).

2.3. Cell printing

2.3.1. Cell culture. L929 murine fibroblast cells were purchased from ATCC and used in this study. The L929 murine fibroblast cells were cultured in the low glucose Dulbecco's

This journal is © The Royal Society of Chemistry 2022

J. Mater. Chem. B, 2022, **10**, 5989–6000 | **5991**

modified eagle medium (DMEM) (Sigma-Aldrich) supplemented with 10% v/v FBS (PAA, GE Healthcare) and 1% v/v antibiotic/antimycotic solution (PAA, GE Healthcare) at a temperature of 37 °C. The culture medium was changed once every three days. The cells were routinely passaged in tissue culture flasks and the adherent cells were harvested using 0.25% trypsin (Sigma-Aldrich) at 90% confluency. Different concentrations of cell-laden bio-inks were prepared; the detached fibroblast cells were suspended in 4% w/v HSP-GelMA bio-inks to obtain the desired cell concentration (0–4 million cells per ml).

2.3.2. Optimal printing cell concentration. 4% H2SP-GelMA bio-inks of varying cell concentrations (0–4 million cells per ml) were printed directly onto 24-well tissue culture plates as 4×4 droplet arrays with a total dispensed volume of 20 nL per spot to evaluate its printability and determine an optimal printable cell concentration. Subsequently, the optimal cell concentration was used for further cell viability and cell proliferation studies.

2.3.3. Cell viability and proliferation. L929 murine fibroblast cells were encapsulated in the 4% H2SP-GelMA bio-ink at an optimal cell concentration of 2 million cells per ml. The cell-laden bio-inks were printed directly onto 24-well tissue culture plates as 4×4 droplet arrays with a total dispensed volume of 20 nL per spot to evaluate the printed cell viability and proliferation profile. The printed 4×4 droplet arrays (sample size, $n = 15$) were crosslinked under the UV light for 130 seconds using a UV flood curing system (Techno Digm, Singapore) and cultured over a period of 7 days. The positive control (2% w/v polyvinylpyrrolidone (PVP) in $1\times$ PBS solution, M_w = 360 kDa – no UV crosslinking is required) and negative control (4% w/v SP-GelMA + 1% w/v PEGDA – UV crosslinking is required) were used in this viability study.

For the cell viability test, the LIVE/DEAD™ viability/cytotoxicity kit (Invitrogen™, Life Technologies, USA) was used to determine the cell viability within each printed group. The cell culture medium was first removed, followed by rinsing the samples with $1\times$ PBS solution for 3 times. Next, the calcein AM solution (stain live cells – green) and ethidium homodimer-1 solution (stain dead cells – red) were added to the different wells and incubated at 37 °C for 20 minutes prior to fluorescence imaging. The samples were observed under an optical/fluorescence microscope (AxioVert.A1, Carl Zeiss, Germany) with 490 nm excitation for live cells and 545 nm excitation for dead cells. The average printed cell viability (%) was obtained by calculating the ratio of viable green cells to dead red cells inside each printed droplet.

For the cell proliferation test, 3 different groups of samples were prepared using the 4% H2SP-GelMA bio-ink containing 2 million cells per ml to the 3D culture environment. The cell-laden 4% H2SP-GelMA bio-inks were (1) manually pipetted (20 μl) onto the 24-well plate cell insert – non-printed group, (2) directly printed (20 μl) onto the 24-well plate cell insert to emulate the 2D culture environment – printed 2D group and (3) directly printed (20 μl) onto a hydrogel layer (4% H2SP-GelMA) inside the 24-well plate cell insert to emulate the 3D culture environment – printed 3D group. All the samples were then crosslinked under the UV light for 130 seconds using a UV flood curing system. PrestoBlue® assay (Invitrogen, Life Technologies, USA) was used to measure the proliferation profile of printed cells encapsulated within the 4% w/v H2SP-GelMA bio-ink based on the relative fluorescence units over a period of 7 days at different time points (day 1, 4 and 7). The fresh culture medium was added to cells prior to the addition of the PrestoBlue® assay (10% of the total volume) in the ratio of $1 : 9$, followed by incubation at 37 °C for 3 hours. A micro-plate reader (SPARK 10M, Tecan) was then used to excite the PrestoBlue® assay at 560 nm wavelength and measure its fluorescence emission at 590 nm wavelength.

Furthermore, scanning electron microscopy (SEM, Jeol JSM-5600LV, Tokyo, Japan) was performed to investigate the morphology of the encapsulated cells within the 4% w/v H2SP-GelMA bio-inks. The samples were first fixed using a 2.5% v/v glutaraldehyde solution (Sigma-Aldrich, USA) at 4 °C for 1 hour, followed by rinsing the samples with distilled water several times to remove the residual glutaraldehyde. Next, the samples were dehydrated using graded ethanol solutions at increasing concentrations (v/v) for at least 10 minutes: 25%, 50%, 70%, 95%, and 100% (twice). After this, samples were washed with distilled water and dried in a desiccator for one day. Lastly, the samples were mounted onto aluminum stubs and gold-coated at 10 mA for 20 seconds before the SEM examination.

2.3.4. Cell patterning. L929 fibroblast cells were stained using a green cytoplasmic membrane dye (CellBrite®, Biotium) and an orange cytoplasmic membrane dye (CellBrite®, Biotium) for cell patterning applications. The cell-laden 4% w/v H2SP-GelMA bio-ink of 2 million cells per ml density was prepared and printed using the thermal inkjet print-heads in the HP D300e digital dispenser.

Two different cell patterning approaches were demonstrated in this work – direct cell patterning and indirect cell patterning. For the direct cell patterning approach, the 4% w/v H2SP-GelMA bio-ink (2 million cells per ml) was printed directly onto 96-well plates to create different patterns. For the indirect cell patterning approach, the 4% w/v H2SP-GelMA bio-ink (0 million cells per ml) was printed on the non-adherent surface to create different patterns for the subsequent cell attachment. The non-adherent surface was prepared by soaking the 24-well plates overnight in a blocking solution comprising 3% w/v bovine serum albumin (BSA, Sigma-Aldrich) and 3% w/v pluronic F-127 (PF-127, Sigma-Aldrich) in $1\times$ PBS solution. The blocking solution was subsequently removed and dried in the oven at 37 °C for at least 24 hours before use. The 4% w/v H2SP-GelMA bio-ink (0 million cells per ml) was then printed over the non-adherent surface and seeded with L929 murine fibroblast cells at a density of 2×10^4 cells per well. All the samples were observed under an optical/fluorescence microscope (AxioVert.A1, Carl Zeiss, Germany).

3. Results and discussion

3.1. Bio-ink synthesis and modification

As highlighted earlier, a major limitation that hinders the prevalent use of material jetting bioprinting approaches is

5992 | *J. Mater. Chem. B*, 2022, **10**, 5989–6000

This journal is © The Royal Society of Chemistry 2022

due to its limited choice of printable bio-inks. In this proof-of-concept study, the gelatin was first functionalized with methacrylic anhydride (MAAh) to obtain photo-curable GelMA bio-inks, followed by a two-step modification process comprising saponification and heat treatment to obtain printable HSP-GelMA bio-inks for thermal inkjet bioprinting (Fig. 1). The high molecular weight gelatin was used in this study as it is a cost-effective and commonly used raw ingredient used in most protocols for GelMA synthesis.[38,58] It yields a higher degree of functionalization[59] and a lower swelling rate as compared to the low molecular weight gelatin.[60] However, the use of lower molecular weight gelatin should be explored for GelMA synthesis in future studies.

Although the SP-GelMA bio-ink (4% w/v concentration) has a shorter polymer chain after partial hydrolysis of methacrylate groups into hydroxyl groups during the saponification process,[61] it demonstrated poor printability in the thermal inkjet print-head as compared to the piezoelectric/electrostatic inkjet print-head. The printing outcome was more like spraying rather than jetting of discrete droplets. Hence, an additional modification is required to further reduce the polymer chain to improve its printability in the thermal inkjet print-head. In this work, a heat treatment, the "autoclaving" process, was implemented to not only further reduce the polymer chain but also improve the sterility of the HSP-GelMA bio-inks for bioprinting applications. The heat treatment process eliminates the presence of micro-organisms by killing bacteria, viruses, and even spores within the bio-ink. The heat treatment process is performed at a high temperature of 121 °C for more than 20 minutes by using saturated steam under at least 15 psi of pressure (or 775 mm of Hg). Different numbers of heat treatment cycles were performed on the SP-GelMA bio-inks to evaluate and obtain HSP-GelMA bio-inks with high printability and consistency.

It is to be noted that thermal degradation might lead to the hydrolysis of peptide bonds;[62,63] hence, it is critical to evaluate the material properties of HSP-GelMA bio-inks after different numbers of heat treatment cycles (0–3 cycles). Hence, different tests (such as bio-ink printability, rheological characterization, UV crosslinking test, nuclear magnetic resonance (NMR) spectroscopy and material swelling ratio) were performed to evaluate and determine the performance of the HSP-GelMA bio-inks. Finally, size-exclusion chromatography with multi-angle light scattering (SEC-MALS) was performed to determine the molecular weight of the HSP-GelMA bio-inks after different heat treatment cycles.

3.2. Bio-ink characterization

The printability of different H×SP-GelMA bio-inks (where × varies from 0 to 3) was evaluated using a thermal inkjet bioprinter (HP D300e Digital Dispenser). The different HSP-GelMA bio-inks were printed as 4 × 4 droplet arrays with a total dispensed volume of 20 nL per spot onto 24-well tissue culture plates. The distinct 4 × 4 droplet arrays were observed in every single well of the 24-well tissue culture plates for H2SP-GelMA and H3SP-GelMA bio-inks, whereas no droplet was observed for H0SP-GelMA and H1SP-GelMA bio-inks. Upon close observation under the optical microscope, numerous satellite droplets were observed in the 24-well tissue culture plates that were printed with H0SP-GelMA and H1SP-GelMA bio-inks (Fig. 2a). Discrete droplets of the H2SP-GelMA bio-ink were printed with the presence of some satellite droplets around the main droplet, and the printing outcome can be further improved by adding viscosity modifiers such as polyvinylpyrrolidone (PVP)[64] and other additives.[65] This observation is corroborated by the rheological characterization results (Fig. 2b), which exhibited a lower bio-ink viscosity with an increasing number of heat treatment cycles. The viscosity of different HSP-GelMA bio-inks decreased from 17.6 mPa s (no heat treatment cycle at a shear rate of 10 000 s^{-1}) to 4.0 mPa s, 3.1 mPa s and 2.8 mPa s after 1, 2 and 3 heat treatment cycles at a shear rate of 10 000 s^{-1} respectively.

Next, the material swelling test showed that the HSP-GelMA bio-inks can absorb significantly more water than the non-modified SP-GelMA bio-ink (Fig. 2c). This observation is corroborated by the compression results in Fig. S1 (ESI†), which showed lower mechanical properties for HSP-GelMA bio-inks. The NMR spectroscopy results in Fig. 2d showed that the HSP-GelMA bio-ink has a lower degree of functionalization (DOF) than the non-modified SP-GelMA. A higher DOF or methacrylate substitution rate leads to a difference in the mechanical strength of GelMA.[59] Notably, the DOF of both H2SP-GelMA and H3SP-GelMA bio-inks decreased by approximately 65%. This resulted in a lower degree of covalent bond crosslinking and UV curing which eventually leads to the lower mechanical strength.[63]

Next, different HSP-GelMA bio-inks (20 μl per sample, $n = 3$) were used to evaluate the influence of heat treatment cycles on the physical and chemical crosslinking properties. The ability to crosslink under standard conditions can be defined as physical crosslinking within 15 minutes when the temperature is below 4 °C and chemical crosslinking within 120 seconds of UV curing duration at 50% intensity. As shown in Table 1, the HSP-GelMA bio-inks that undergo 2 or more heat treatment cycles (H2SP-GelMA and H3SP-GelMA) could not undergo physical or chemical crosslinking under standard conditions. Notably, the H2SP-GelMA bio-ink can be chemically crosslinked when the UV curing duration is extended to at least 130 seconds, whereas the H3SP-GelMA bio-ink could not be chemically crosslinked at a longer crosslinking time (>180 seconds) prior to the sample drying. This was further confirmed by the temperature sweep test of the H3SP-GelMA bio-ink as shown in Fig. 3, which showed that the storage modulus (G') is lower than the loss modulus (G'') – hence the H3SP-GelMA bio-ink remained in the liquid state as there is no cross-over point of storage and loss modulus even at lower temperatures. Furthermore, it has been reported that a longer UV crosslinking duration will lead to a lower cell viability.[66] Thus, H3SP-GelMA is not suitable for cell bioprinting applications.

Finally, it is confirmed that the two-step modification process comprising saponification and heat treatment can shorten the molecular chain which leads to a lower weight average molecular weight (M_w) and number average molar mass (M_n)

This journal is © The Royal Society of Chemistry 2022

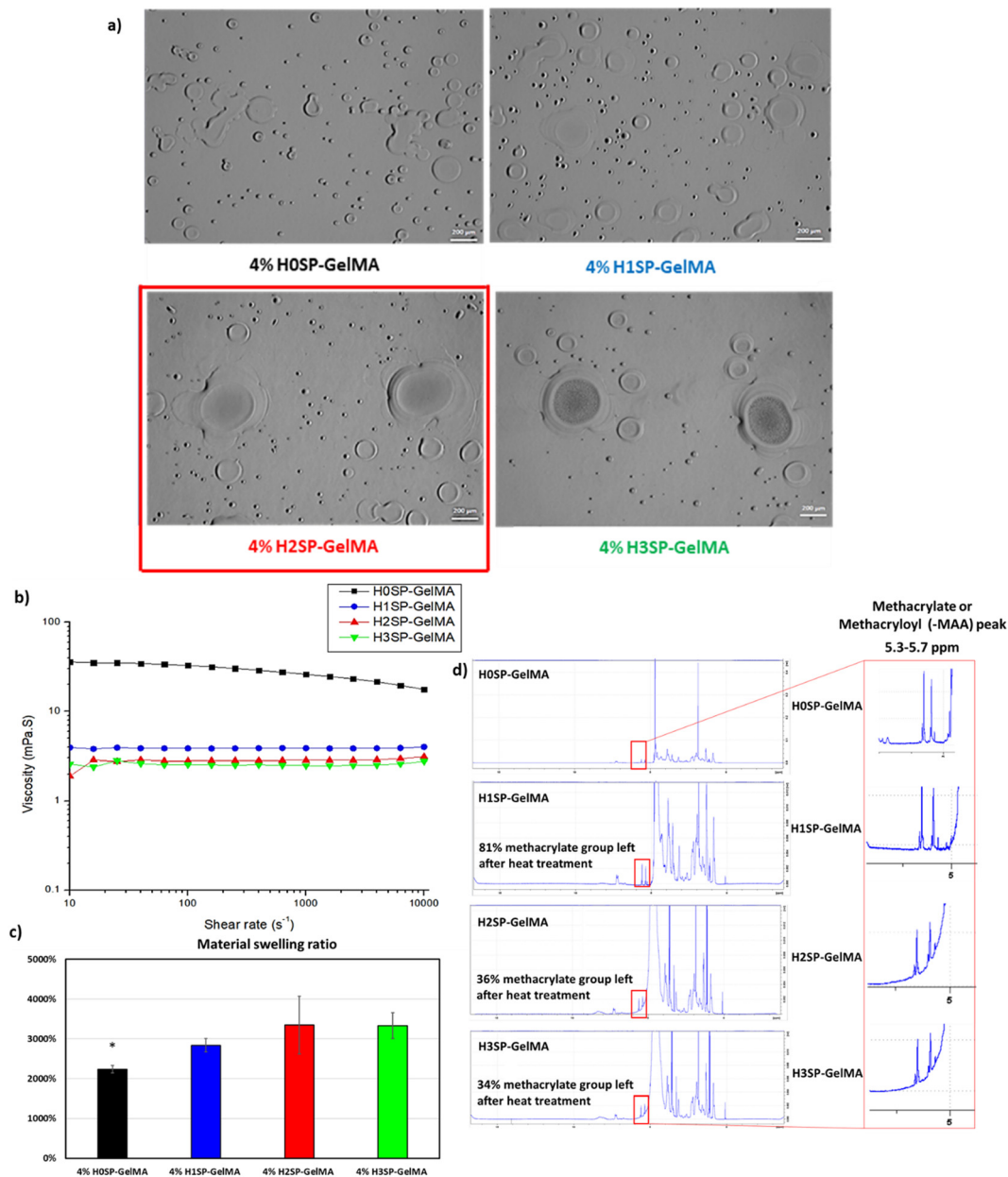J. Mater. Chem. B, 2022, **10**, 5989–6000 | **5993**

Fig. 2 (a) Bio-ink printability test – different HSP-GelMA bio-inks were used to print droplet arrays onto 24-well plates. (b) Rheological characterization of different HSP-GelMA bio-inks at varying shear rates from 10 to 10 000 s^{-1} to evaluate the viscosity of the bio-inks. (c) Material swelling test of different HSP-GelMA bio-inks to evaluate its water uptake ability. (d) NMR spectroscopy results of different HSP-GelMA bio-inks to determine the degree of functionalized (DOF) groups after heat treatment cycles.

Table 1 Influence of heat treatment cycles on the physical and chemical crosslinking properties

Bio-inks	Physical crosslinking (<4 °C within 15 min)	Chemical crosslinking (50% intensity and 120 seconds)
H0SP-GelMA	✔	✔
H1SP-GelMA	✔	Δ
H2SP-GelMA	Δ	Δ
H3SP-GelMA	✗	✗

✔ = Crosslink under standard conditions, Δ = partial crosslink under standard conditions, ✗ = do not crosslink under standard conditions.

based on the result from SEC-MALS in Table 2. The saponification process reduced the molecular weight by almost 40% from the original M_w in GelMA. The heat treatment further reduced the M_w from SP-GelMA by approximately 35% and that is the range of the molecular weight that can dispense by thermal inkjet at a 4% w/v concentration. The significant error and large polydispersity in both H1SP-GelMA and H2SP-GelMA were due to the additional hydrolysis process which leads to a huge difference in the length of the polymer chain (molecular weight) and side chains of the polymer. As such, the printability of the GelMA bio-inks in the thermal inkjet printer is
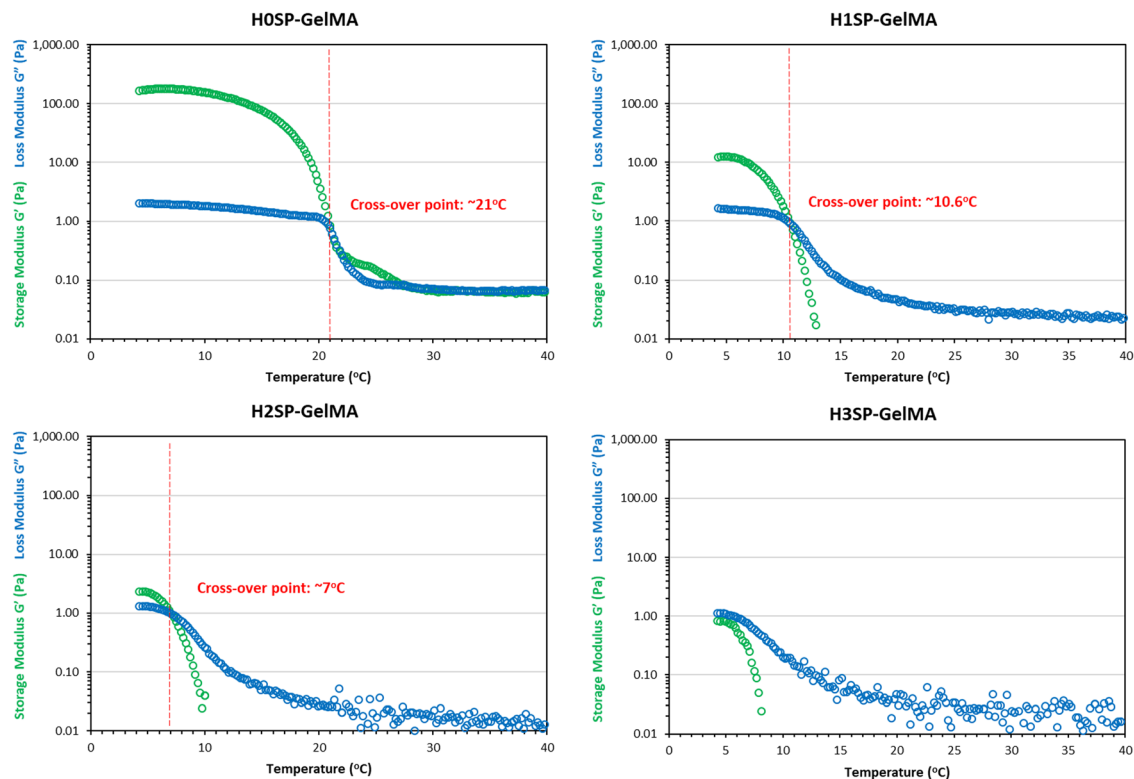
5994 | *J. Mater. Chem. B*, 2022, **10**, 5989–6000

This journal is © The Royal Society of Chemistry 2022

Fig. 3 Temperature sweep analysis of different HSP-GelMA bio-inks from 4 °C to 40 °C to determine the cross-over point of the storage modulus (G') and loss modulus (G'').

Table 2 Influence of heat treatment on the SEC-MALS results of different HSP-GelMA bio-inks

Bio-inks	M_{w} (kDa)	M_{n} (kDa)	Error (%)	Polydispersity ($M_{\mathrm{w}}/M_{\mathrm{n}}$)
4%Pristine GelMA	224.30	209.43	5.00	1.07
4% H0SP-GelMA	142.20	136.34	3.60	1.04
4% H1SP-GelMA	49.70	25.80	6.90	1.93
4% H2SP-GelMA	31.60	23.44	27.70	1.35

significantly improved after the saponification process and an optimal cycle of 2 heat treatment processes. In the subsequent experiments, H2SP-GelMA bio-inks were used to investigate the influence of cells on the bio-inks.

3.3. Cell printing

4% H2SP-GelMA bio-inks of varying cell concentrations (0–4 million cells per ml) were printed directly onto 24-well tissue culture plates as 4 × 4 droplet arrays with a total dispensed volume of 60 nL per spot to evaluate its printability and determine an optimal printable cell concentration. It was noted that the 4% H2SP-GelMA bio-ink with a higher cell concentration would lead to poor droplet positioning accuracy as depicted by the droplet shape in Fig. 4a. When the droplet positioning accuracy is high, the dispensed droplets would coalesce and form a large, rounded droplet at the pre-defined position as observed in a lower cell concentration. In contrast,
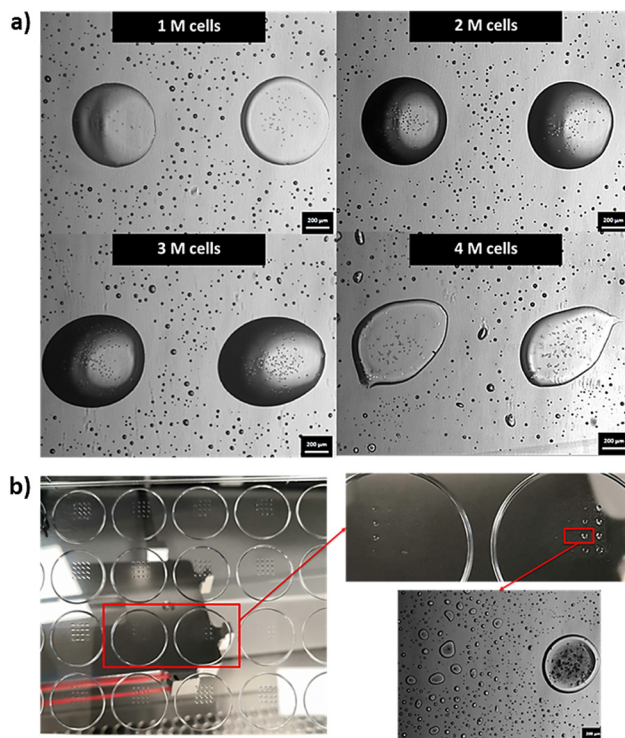

Fig. 4 (a) Influence of the cell concentration on the printability of 4% w/v H2SP-GelMA bio-inks; scale bar = 200 μm. (b) Representative images of deposited droplets on tissue culture well plates; the increased probability of nozzle clogging occurs at higher cell concentrations (missing droplet on the left hand side as shown in the enlarged image).

This journal is © The Royal Society of Chemistry 2022

J. Mater. Chem. B, 2022, **10**, 5989–6000 | **5995**

the dispensed droplets are positioned further apart and exhibited a stretched and elongated droplet morphology at the low droplet positioning accuracy. Furthermore, the probability of nozzle clogging increases at the high cell concentration (3–4 million cells per ml) and typically occurs after printing approximately $\sim$70% of the total volume (Fig. 4b). Hence, an optimal cell concentration of 2 million cells per ml is selected for the 4% H2SP-GelMA bio-ink to achieve higher droplet positioning accuracy and mitigate the occurrence of potential nozzle clogging.

Next, the viability of printed cells was evaluated over a period of 7 days using three different types of bio-inks (a constant cell concentration of 2 million cells per ml) which include the 4% H2SP-GelMA bio-ink, a positive control group (2% w/v polyvinylpyrrolidone (PVP) in 1$\times$ PBS solution, M_w = 360 kDa – no UV crosslinking is required)[64] and a negative control group (4% w/v SP-GelMA + 1% w/v PEGDA – UV crosslinking is required)[67] (Fig. 5a). The positive control group has

the highest cell viability over a period of 7 days; its cell viability ranges from 99.5 $\pm$ 0.51% on day 0 to 99.8 $\pm$ 0.03% on day 7. Conversely, both the H2SP-GelMA bio-ink and the negative control group have significantly lower cell viabilities of 74.5 $\pm$ 4.98% and 62.8 $\pm$ 3.82% on day 0, respectively. This can be attributed to the UV crosslinking process which induced cell damage to the encapsulated L929 fibroblast cells and resulted in lower initial cell viability.[68] Notably, the viability of printed cells in the 4% H2SP-GelMA bio-ink increased gradually from 74.5 $\pm$ 4.98% on day 0 to 96.8 $\pm$ 0.77% on day 7, whereas the viability of printed cells in the negative control group decreased gradually from 62.8 $\pm$ 3.82% on day 0 to 47.5 $\pm$ 8.33% on day 7.

Further studies were performed to evaluate the influence of printing and 2D *vs.* 3D culture environment on the cell proliferation profile. Three different groups of samples were prepared using the 4% H2SP-GelMA bio-ink containing 2 million cells per ml – (1) non-printed group, (2) printed 2D cell culture environment and (3) printed 3D cell culture environment.
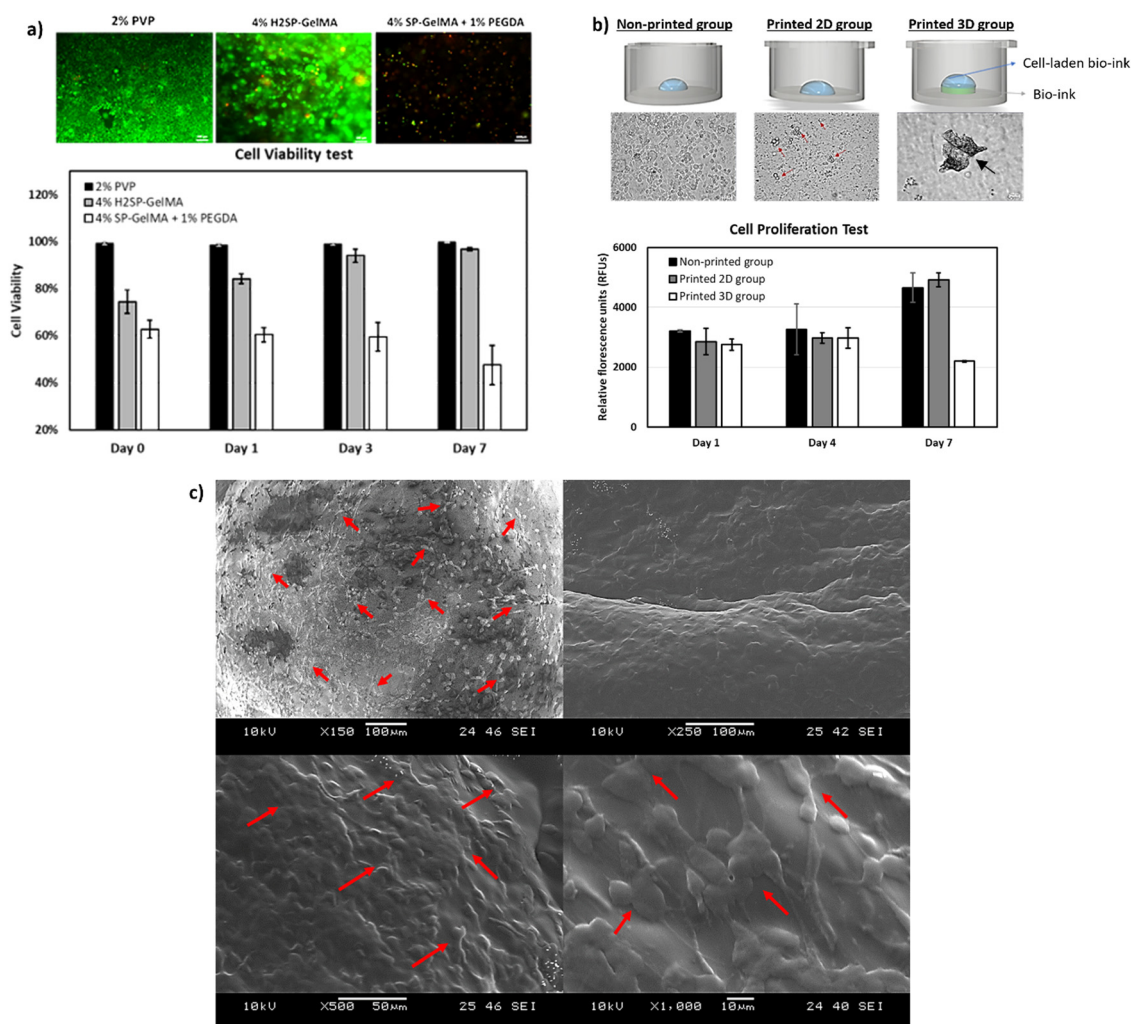

Fig. 5 (a) Representative images of live-dead staining (2% w/v PVP bio-ink – positive control, 4% HSP-GelMA bio-ink and 4% SP-GelMA + 1% PEGDA bio-ink – negative control) on day 7 – live cells were stained green and dead cells were stained red. (b) Evaluation of the cell proliferation profile over a period of 7 days using the PrestoBlue assay – the non-printed group *vs.* the printed 2D group *vs.* the printed 3D group. (c) Representative SEM images showing the morphology of encapsulated cells within the 4% w/v HSP-GelMA bio-ink samples on day 7.

5996 | *J. Mater. Chem. B*, 2022, **10**, 5989–6000

This journal is © The Royal Society of Chemistry 2022

The results showed that there is no significant difference in the cell proliferation profile on day 1; the cells remained viable and continued growing gradually over a period of 7 days. It was observed that there is a significant increase in measured relative fluorescence units (RFUs) for the non-printed group and printed 2D cell culture environment on day 7 as the encapsulated cells migrated out of the UV-crosslinked 4% H2SP-GelMA bio-inks and were growing on the well plate. In contrast, the cells in the printed 3D cell culture environment were observed to form numerous 3D cell spheroids on day 7 and exhibited a slower proliferation rate (Fig. 5b). The spheroid-forming phenomenon exhibited by the L929 cells within the 3D cell culture environment will be investigated in future studies. Further SEM analysis of the 4% H2SP-GelMA bio-inks on day 7 showed that the encapsulated L929 cells were uniformly distributed across the crosslinked bio-inks (as indicated by the red arrows) and proliferating well (Fig. 5c). Hence, the 4% H2SP-GelMA bio-ink can be considered a biocompatible bio-ink that supports cell encapsulation and proliferation over time based on the cell viability and proliferation results.

Two different cell patterning approaches were demonstrated in this work – direct cell patterning and indirect cell patterning. For the direct cell patterning approach, the cell-laden 4% H2SP-GelMA bio-ink was directly printed on the 96-well plates to create the pattern as shown in Fig. 6a (outer droplets containing the green cells and inner droplets containing the red cells). The 4% H2SP-GelMA bio-ink with an optimal cell concentration of 2 million cells per ml resulted in high droplet positioning accuracy and facilitated the precise patterning of the green and red cells at their pre-defined positions (Fig. 6a). The ability to perform cell patterning is critical for fundamental studies of cell–cell interactions, such as the interactions between the human dermal fibroblasts and endothelium cells for potential vascularization.[69]

Next, the indirect cell patterning approach was performed by printing the 4% H2SP-GelMA bio-ink (0 million cells per ml) directly onto the blocking well plate (Fig. 6b). An optional step such as printing of 3% w/v pluronic F-127 around the boundary of the H2SP-GelMA bio-ink can be performed to mitigate the potential cell attachment at the undesirable regions. Most of the seeded cells were found within the defined regions; the
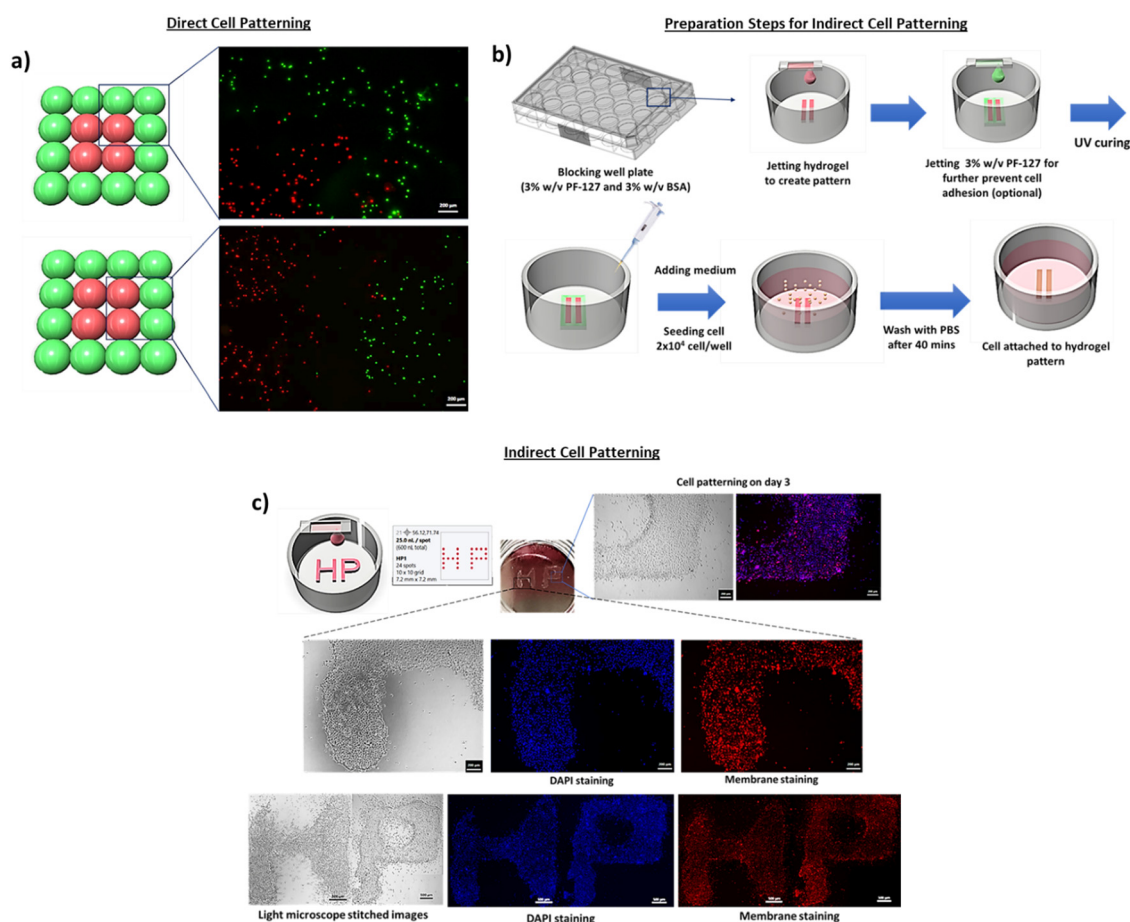

Fig. 6 (a) Direct cell patterning using 4% H2SP-GelMA bio-inks with encapsulated L929 murine fibroblast cells at 2 million cells per ml with scale bar = 200 μm. (b) Schematic drawing of preparation steps for indirect cell patterning. (c) (Top) Optical and fluorescence images of indirect cell patterning with seeded L929 murine fibroblast cells at different positions on day 3 – scale bar = 200 μm. (Bottom) Optical and fluorescence stitched images of the HP logo with scale bar = 500 μm.

This journal is © The Royal Society of Chemistry 2022

J. Mater. Chem. B, 2022, 10, 5989–6000 | 5997

cells were well-aligned and formed the "HP" pattern within 3 days as indicated by both optical and fluorescence stitched images (Fig. 6c). This particular indirect cell patterning approach eliminates the need for a specific photo-mask and PDMS stamp in the conventional stamping technique.[70] Furthermore, the 3D bioprinting technique does not require a multi-step of chemical bonding such as plasma treatment or protein immobilization.[71] Hence, the material jetting bioprinting technique is a facile approach for fundamental cell–cell and cell–material interaction studies.

4. Conclusion

In this work, a two-step modification process comprising saponification and heat treatment was performed; the GelMA bio-ink was first modified *via* the saponification process under highly alkali conditions to obtain saponified GelMA (SP-GelMA), followed by heat treatment *via* the autoclaving process to obtain heat-treated SP-GelMA (HSP-GelMA). An optimal heat treatment process of 2 cycles resulted in a significant decrease in the viscosity of the bio-ink and the molecular weight, while maintaining its ability to undergo both physical and chemical crosslinking, hence improving the printability of photo-curable 4% H2SP-GelMA bio-inks in the thermal inkjet print-head. The 4% H2SP-GelMA bio-inks demonstrated good biocompatibility properties as shown in the cell viability test, cell proliferation test and SEM analysis. Nevertheless, the mechanical properties of the 4% H2SP-GelMA bio-inks have decreased drastically compared to those of the non-modified SP-GelMA due to its low concentration (4% w/v) and hydrolysis of peptide bonds. Further studies can be performed in the future to further enhance its overall mechanical strength *via* combination with other suitable bio-inks. The two-step bio-ink modification process developed in this work is a facile method to produce printable hydrogel-based bio-inks for thermal inkjet bioprinting that can be potentially used for fundamental cell–cell and cell–material interaction studies.

Conflicts of interest

The authors declare no potential conflicts of interest.

Acknowledgements

References

1 W. L. Ng, C. K. Chua and Y.-F. Shen, Print Me An Organ! Why We Are Not There Yet, *Prog. Polym. Sci.*, 2019, **97**, 101145.

2 W. Sun, B. Starly, A. C. Daly, J. A. Burdick, J. Groll, G. Skeldon, W. Shu, Y. Sakai, M. Shinohara, M. Nishikawa, J. Jang, D.-W. Cho, M. Nie, S. Takeuchi, S. Ostrovidov, A. Khademhosseini, R. D. Kamm, V. Mironov, L. Moroni and I. T. Ozbolat, The bioprinting roadmap, *Biofabrication*, 2020, **12**(2), 022002.

3 R. Levato, T. Jungst, R. G. Scheuring, T. Blunk, J. Groll and J. Malda, From shape to function: the next step in bioprinting, *Adv. Mater.*, 2020, **32**(12), 1906423.

4 J. M. Lee, W. L. Ng and W. Y. Yeong, Resolution and shape in bioprinting: Strategizing towards complex tissue and organ printing, *Appl. Phys. Rev*, 2019, **6**(1), 011307.

5 W. L. Ng, A. Chan, Y. S. Ong and C. K. Chua, Deep learning for fabrication and maturation of 3D bioprinted tissues and organs, *Virtual Phys Prototyp*, 2020, **15**(3), 340–358.

6 J. He, M. Mao, X. Li and C. K. Chua, Bioprinting of 3D Functional Tissue Constructs, *Int. J. Bioprint.*, 2021, **7**(3), 1–2.

7 R. Suntornnond, J. An and C. K. Chua, Bioprinting of thermoresponsive hydrogels for next generation tissue engineering: a review, *Macromol. Mater. Eng.*, 2017, **302**(1), 1600266.

8 W. L. Ng, S. Wang, W. Y. Yeong and M. W. Naing, Skin bioprinting: impending reality or fantasy?, *Trends Biotechnol.*, 2016, **34**(9), 689–699.

9 S. Patra and V. Young, A review of 3D printing techniques and the future in biofabrication of bioprinted tissue, *Cell Biochem. Biophys.*, 2016, **74**(2), 93–98.

10 S. V. Murphy and A. Atala, 3D bioprinting of tissues and organs, *Nat. Biotechnol.*, 2014, **32**(8), 773–785.

11 R. E. Saunders and B. Derby, Inkjet printing biomaterials for tissue engineering: bioprinting, *Int. Mater. Rev.*, 2014, **59**(8), 430–448.

12 W. L. Ng, X. Huang, V. Shkolnikov, G. L. Goh, R. Suntornnond and W. Y. Yeong, Controlling Droplet Impact Velocity and Droplet Volume: Key Factors to Achieving High Cell Viability in Sub-Nanoliter Droplet-based Bioprinting, *Int. J. Bioprint.*, 2022, **8**(1), 424.

13 W. L. Ng, W. Y. Yeong and M. W. Naing, Microvalve bioprinting of cellular droplets with high resolution and consistency, *Proceedings of the 2nd International Conference on Progress in Additive Manufacturing*, 2016, pp. 397–402.

14 L. Koch, O. Brandt, A. Deiwick and B. Chichkov, Laser assisted bioprinting at different wavelengths and pulse durations with a metal dynamic release layer: A parametric study, *Int. J. Bioprint.*, 2017, **3**(1), 42–53.

15 F. Guo, P. Li, J. B. French, Z. Mao, H. Zhao, S. Li, N. Nama, J. R. Fick, S. J. Benkovic and T. J. Huang, Controlling cell–cell interactions using surface acoustic waves, *Proc. Natl. Acad. Sci. U. S. A.*, 2015, **112**(1), 43–48.

16 Y. E. Choe and G. H. Kim, A PCL/cellulose coil-shaped scaffold via a modified electrohydrodynamic jetting process, *Virtual Phys Prototyp*, 2020, **15**(4), 403–416.

5998 | *J. Mater. Chem. B*, 2022, **10**, 5989–6000

This journal is © The Royal Society of Chemistry 2022

17 I. T. Ozbolat and M. Hospodiuk, Current advances and future perspectives in extrusion-based bioprinting, *Biomaterials*, 2016, **76**, 321–343.

18 P. Zhuang, W. L. Ng, J. An, C. K. Chua and L. P. Tan, Layer-by-layer ultraviolet assisted extrusion-based (UAE) bioprinting of hydrogel constructs with high aspect ratio for soft tissue engineering applications, *PLoS One*, 2019, **14**(6), e0216776.

19 W. L. Ng, W. Y. Yeong and M. W. Naing, Potential of Bioprinted Films for Skin Tissue Engineering, Proceedings of the 1st International Conference on Progress in Additive Manufacturing (2014) 441–446.

20 Z. Meng, J. He, J. Li, Y. Su and D. Li, Melt-based, solvent-free additive manufacturing of biodegradable polymeric scaffolds with designer microstructures for tailored mechanical/biological properties and clinical applications, *Virtual Phys Prototyp*, 2020, **15**(4), 417–444.

21 W. L. Ng, J. M. Lee, M. Zhou, Y.-W. Chen, K.-X. A. Lee, W. Y. Yeong and Y.-F. Shen, Vat polymerization-based bioprinting–process, materials, applications and regulatory challenges, *Biofabrication*, 2020, **12**(2), 022001.

22 W. Li, L. S. Mille, J. A. Robledo, T. Uribe, V. Huerta and Y. S. Zhang, Recent Advances in Formulating and Processing Biomaterial Inks for Vat Polymerization-Based 3D Printing, *Adv. Healthc. Mater.*, 2020, **9**(15), 2000156.

23 D. Nieto, J. A. Marchal Corrales, A. Jorge de Mora and L. Moroni, Fundamentals of light-cell–polymer interactions in photo-cross-linking based bioprinting, *APL Bioeng.*, 2020, **4**(4), 041502.

24 X. Li, B. Liu, B. Pei, J. Chen, D. Zhou, J. Peng, X. Zhang, W. Jia and T. Xu, Inkjet Bioprinting of Biomaterials, *Chem. Rev.*, 2020, **120**(19), 10793–10833.

25 W. L. Ng, J. M. Lee, W. Y. Yeong and M. Win Naing, Microvalve-based bioprinting – process, bio-inks and applications, *Biomater. Sci.*, 2017, **5**(4), 632–647.

26 V. Yusupov, S. Churbanov, E. Churbanova, K. Bardakova, A. Antoshin, S. Evlashin, P. Timashev and N. Minaev, Laser-induced forward transfer hydrogel printing: a defined route for highly controlled process, *Int. J. Bioprint.*, 2020, **6**(3), 271.

27 H. Gudupati, M. Dey and I. Ozbolat, A Comprehensive Review on Droplet-based Bioprinting: Past, Present and Future, *Biomaterials*, 2016, **102**, 20–42.

28 W. L. Ng, Z. Q. Tan, W. Y. Yeong and M. W. Naing, Proof-of-concept: 3D bioprinting of pigmented human skin constructs, *Biofabrication*, 2018, **10**(2), 1–13 025005.

29 W. L. Ng and W. Y. Yeong, The Future of Skin Toxicology Testing - 3D Bioprinting Meets Microfluidics, *Int. J. Bioprint.*, 2019, **5**(2.1), 237.

30 S. Agarwala, J. M. Lee, W. L. Ng, M. Layani, W. Y. Yeong and S. Magdassi, A novel 3D bioprinted flexible and biocompatible hydrogel bioelectronic platform, *Biosens. Bioelectron.*, 2018, **102**, 365–371.

31 W. L. Ng, T. C. Ayi, Y.-C. Liu, S. L. Sing, W. Y. Yeong and B.-H. Tan, Fabrication and Characterization of 3D Bioprinted Triple-layered Human Alveolar Lung Models, *Int. J. Bioprint.*, 2021, **7**(2), 332.

32 W. L. Ng, J. M. Lee, M. Zhou and W. Y. Yeong, Hydrogels for 3-D bioprinting-based tissue engineering, in *Rapid Prototyping of Biomaterials*, ed. R. Narayan, Elsevier, Chapel Hill, NC, 2020, pp. 183–204.

33 S. C. Pedroza-González, M. Rodriguez-Salvador, B. E. Pérez-Benítez, M. M. Alvarez and G. Trujillo-de Santiago, Bioinks for 3D Bioprinting: A Scientometric Analysis of Two Decades of Progress, *Int. J. Bioprint.*, 2021, **7**(2), 68–91.

34 N. Noor, A. Shapira, R. Edri, I. Gal, L. Wertheim and T. Dvir, 3D Printing of Personalized Thick and Perfusable Cardiac Patches and Hearts, *Adv. Sci.*, 2019, **6**(11), 1900344.

35 E. O. Osidak, V. I. Kozhukhov, M. S. Osidak and S. P. Domogatsky, Collagen as Bioink for Bioprinting: A Comprehensive Review, *Int. J. Bioprint.*, 2020, **6**(3), 270.

36 J. M. Lee, S. K. Q. Suen, W. L. Ng, W. C. Ma and W. Y. Yeong, Bioprinting of Collagen: Considerations, Potentials, and Applications, *Macromol. Biosci.*, 2020, **21**(1), 2000280.

37 W. L. Ng, M. H. Goh, W. Y. Yeong and M. W. Naing, Applying Macromolecular Crowding to 3D Bioprinting: Fabrication of 3D Hierarchical Porous Collagen-based Hydrogel Constructs, *Biomater. Sci.*, 2018, **6**(3), 562–574.

38 J. W. Nichol, S. T. Koshy, H. Bae, C. M. Hwang, S. Yamanlar and A. Khademhosseini, Cell-laden microengineered gelatin methacrylate hydrogels, *Biomaterials*, 2010, **31**(21), 5536–5544.

39 L. E. Bertassoni, J. C. Cardoso, V. Manoharan, A. L. Cristino, N. S. Bhise, W. A. Araujo, P. Zorlutuna, N. E. Vrana, A. M. Ghaemmaghami and M. R. Dokmeci, Direct-write bioprinting of cell-laden methacrylated gelatin hydrogels, *Biofabrication*, 2014, **6**(2), 1–11 024105.

40 W. L. Ng, W. Y. Yeong and M. W. Naing, Development of Polyelectrolyte Chitosan-gelatin Hydrogels for Skin Bioprinting, *Procedia CIRP*, 2016, **49**, 105–112.

41 W. L. Ng, W. Y. Yeong and M. W. Naing, Polyelectrolyte gelatin-chitosan hydrogel optimized for 3D bioprinting in skin tissue engineering, *Int. J. Bioprint.*, 2016, **2**(1), 53–62.

42 I. Frisman, D. Seliktar and H. Bianco-Peled, Nanostructuring PEG-fibrinogen hydrogels to control cellular morphogenesis, *Biomaterials*, 2011, **32**(31), 7839–7846.

43 Y. B. Lee, S. Polio, W. Lee, G. Dai, L. Menon, R. S. Carroll and S. S. Yoo, Bio-printing of collagen and VEGF-releasing fibrin gel scaffolds for neural stem cell culture, *Exp. Neurol.*, 2010, **223**(2), 645–652.

44 S. Stichler, T. Böck, N. Paxton, S. Bertlein, R. Levato, V. Schill, W. Smolan, J. Malda, J. Teßmar and T. Blunk, Double printing of hyaluronic acid/poly (glycidol) hybrid hydrogels with poly (ε-caprolactone) for MSC chondrogenesis, *Biofabrication*, 2017, **9**(4), 1–12 044108.

45 M. T. Poldervaart, B. Goversen, M. De Ruijter, A. Abbadessa, F. P. Melchels, F. C. Öner, W. J. Dhert, T. Vermonden and J. Alblas, 3D bioprinting of methacrylated hyaluronic acid (MeHA) hydrogel with intrinsic osteogenicity, *PLoS One*, 2017, **12**(6), e0177628.

46 X. Zhang, Y. Liu, Q. Zuo, Q. Wang, Z. Li, K. Yan, T. Yuan, Y. Zhang, K. Shen and R. Xie, 3D Bioprinting of Biomimetic Bilayered Scaffold Consisting of Decellularized Extracellular

This journal is © The Royal Society of Chemistry 2022

J. Mater. Chem. B, 2022, **10**, 5989–6000 | 5999

Matrix and Silk Fibroin for Osteochondral Repair, *Int. J. Bioprint.*, 2021, **7**(4), 85–98.

47 S. H. Kim, Y. K. Yeon, J. M. Lee, J. R. Chao, Y. J. Lee, Y. B. Seo, M. T. Sultan, O. J. Lee, J. S. Lee and S.-I. Yoon, Precisely printable and biocompatible silk fibroin bioink for digital light processing 3D printing, *Nat. Commun*, 2018, **9**(1), 1620.

48 D. Chimene, R. Kaunas and A. K. Gaharwar, Hydrogel Bioink Reinforcement for Additive Manufacturing: A Focused Review of Emerging Strategies, *Adv. Mater.*, 2020, **32**(1), 1902026.

49 G. Ying, N. Jiang, C. Yu and Y. S. Zhang, Three-dimensional bioprinting of gelatin methacryloyl (GelMA), *Bio-Design and Manufacturing*, 2018, **1**(4), 215–224.

50 E. Y. Tan, R. Suntornnond and W. Y. Yeong, High-Resolution Novel Indirect Bioprinting of Low-Viscosity Cell-Laden Hydrogels via Model-Support Bioink Interaction, *3D Print. Addit. Manuf.*, 2021, **8**(1), 69–78.

51 K. Yue, G. Trujillo-de Santiago, M. M. Alvarez, A. Tamayol, N. Annabi and A. Khademhosseini, Synthesis, properties, and biomedical applications of gelatin methacryloyl (GelMA) hydrogels, *Biomaterials*, 2015, **73**, 254–271.

52 R. Suntornnond, E. Y. S. Tan, J. An and C. K. Chua, A highly printable and biocompatible hydrogel composite for direct printing of soft and perfusable vasculature-like structures, *Sci. Rep.*, 2017, **7**(1), 1–11 16902.

53 I. Pepelanova, K. Kruppa, T. Scheper and A. Lavrentieva, Gelatin-Methacryloyl (GelMA) Hydrogels with Defined Degree of Functionalization as a Versatile Toolkit for 3D Cell Culture and Extrusion Bioprinting, *Bioengineering*, 2018, **5**(3), 55.

54 D. Jang, D. Kim and J. Moon, Influence of fluid physical properties on ink-jet printability, *Langmuir*, 2009, **25**(5), 2629–2635.

55 C. Xu, M. Zhang, Y. Huang, A. Ogale, J. Fu and R. R. Markwald, Study of droplet formation process during drop-on-demand inkjetting of living cell-laden bioink, *Langmuir*, 2014, **30**(30), 9130–9138.

56 C. Meinert, C. Theodoropoulos, T. J. Klein, D. W. Hutmacher and D. Loessner, A method for prostate and breast cancer cell spheroid cultures using gelatin methacryloyl-based hydrogels, *Prostate Cancer*, Springer, 2018, pp. 175–194.

57 S. Yoon, J. A. Park, H. R. Lee, W. H. Yoon, D. S. Hwang and S. Jung, Inkjet–spray hybrid printing for 3D freeform fabrication of multilayered hydrogel structures, *Adv. Healthc. Mater.*, 2018, **7**(14), 1800050.

58 D. Loessner, C. Meinert, E. Kaemmerer, L. C. Martine, K. Yue, P. A. Levett, T. J. Klein, F. P. Melchels, A. Khademhosseini and D. W. Hutmacher, Functionalization, preparation and use of cell-laden gelatin methacryloyl–based hydrogels as modular tissue culture platforms, *Nat. Protoc.*, 2016, **11**(4), 727–746.

59 M. Zhu, Y. Wang, G. Ferracci, J. Zheng, N.-J. Cho and B. H. Lee, Gelatin methacryloyl and its hydrogels with an exceptional degree of controllability and batch-to-batch consistency, *Sci. Rep.*, 2019, **9**(1), 6863.

60 H. T. Peng, L. Martineau and P. N. Shek, Hydrogel-elastomer composite biomaterials: 3. Effects of gelatin molecular weight and type on the preparation and physical properties of inter-penetrating polymer networks, *J. Mater. Sci.: Mater. Med.*, 2008, **19**(3), 997–1007.

61 J. Zheng, M. Zhu, G. Ferracci, N.-J. Cho and B. H. Lee, Hydrolytic Stability of Methacrylamide and Methacrylate in Gelatin Methacryloyl and Decoupling of Gelatin Methacryl-amide from Gelatin Methacryloyl through Hydrolysis, *Macromol. Chem. Phys.*, 2018, **219**(18), 1800266.

62 C. D. O'Connell, C. Onofrillo, S. Duchi, X. Li, Y. Zhang, P. Tian, L. Lu, A. Trengove, A. Quigley, S. Gambhir, A. Khansari, T. Mladenovska, A. O'Connor, C. Di Bella, P. F. Choong and G. G. Wallace, Evaluation of sterilisation methods for bio-ink components: gelatin, gelatin methacry-loyl, hyaluronic acid and hyaluronic acid methacryloyl, *Biofabrication*, 2019, **11**(3), 035003.

63 M. Rizwan, S. W. Chan, P. A. Comeau, T. L. Willett and E. K. Yim, Effect of sterilization treatment on mechanical properties, biodegradation, bioactivity and printability of GelMA hydrogels, *Biomed. Mater.*, 2020, **15**(6), 065017.

64 W. L. Ng, W. Y. Yeong and M. W. Naing, Polyvinyl-pyrrolidone-Based Bio-Ink Improves Cell Viability and Homogeneity during Drop-On-Demand Printing, *Materials*, 2017, **10**(2), 1–12 190.

65 S. M. Z. Hossain, R. E. Luckham, A. M. Smith, J. M. Lebert, L. M. Davies, R. H. Pelton, C. D. M. Filipe and J. D. Brennan, Development of a Bioactive Paper Sensor for Detection of Neurotoxins Using Piezoelectric Inkjet Printing of Sol−Gel-Derived Bioinks, *Anal. Chem.*, 2009, **81**(13), 5474–5483.

66 T. U. Nguyen, K. E. Watkins and V. Kishore, Photochemi-cally crosslinked cell-laden methacrylated collagen hydro-gels with high cell viability and functionality, *J. Biomed. Mater. Res. A*, 2019, **107**(7), 1541–1550.

67 D. Perera, M. Medini, D. Seethamraju, R. Falkowski, K. White and R. M. Olabisi, The effect of polymer molecular weight and cell seeding density on viability of cells entrapped within PEGDA hydrogel microspheres, *J. Micro-encapsulation*, 2018, **35**(5), 475–481.

68 R. Masuma, S. Kashima, M. Kurasaki and T. Okuno, Effects of UV wavelength on cell damages caused by UV irradia-tion in PC12 cells, *J. Photochem. Photobiol., B*, 2013, **125**, 202–208.

69 R. Costa-Almeida, M. Gomez-Lazaro, C. Ramalho, P. L. Granja, R. Soares and S. G. Guerreiro, Fibroblast-Endothelial Partners for Vascularization Strategies in Tissue Engineering, *Tissue Engineering Part A*, 2014, **21**(5–6), 1055–1065.

70 S.-i Funano, N. Tanaka and Y. Tanaka, User-friendly cell patterning methods using a polydimethylsiloxane mold with microchannels, *Dev., Growth Differ.*, 2020, **62**(3), 167–176.

71 A. Shakeri, S. M. Imani, E. Chen, H. Yousefi, R. Shabbir and T. F. Didar, Plasma-induced covalent immobilization and patterning of bioactive species in microfluidic devices, *Lab Chip*, 2019, **19**(18), 3104–3115.

6000 | *J. Mater. Chem. B*, 2022, **10**, 5989–6000

This journal is © The Royal Society of Chemistry 2022